

SWIFT OBSERVATIONS OF SMC X-3 DURING ITS 2016 SUPER-EDDINGTON OUTBURST

SHAN-SHAN WENG¹, MING-YU GE², HAI-HUI ZHAO¹, WEI WANG³, SHUANG-NAN ZHANG², WEI-HAO BIAN¹, QI-RONG YUAN¹

¹ Department of Physics and Institute of Theoretical Physics, Nanjing Normal University, Nanjing 210023, China

² Key Laboratory of Particle Astrophysics, Institute of High Energy Physics, Chinese Academy of Sciences, Beijing 100049, China and

³ National Astronomical Observatories, Chinese Academy of Sciences, Beijing 100012, China

Draft version January 12, 2017

ABSTRACT

The Be X-ray pulsar, SMC X-3 underwent a giant outburst in 2016, which was monitored with the *Swift* satellite. During the outburst, the fluxes in the broadband increased dramatically, and the 0.6–10 keV unabsorbed luminosity reached an extreme value of $\sim 10^{39}$ erg/s around August 24. Using the *Swift/XRT* data, we measure the observed pulse frequency of neutron star to compute the orbital elements of the binary. After applying the orbital corrections to *Swift* observations, we find that the spin frequency increases steadily from 128.02 mHz on August 10 and becomes close to the spin equilibrium ~ 128.73 mHz at the late time ($L_X \sim 2.3 \times 10^{37}$ erg/s), indicating a strong magnetic field of neutron star $B \sim 7.3 \times 10^{12}$ G. The spin-up rate is tightly correlated with the X-ray luminosity during the super-Eddington outburst. The pulse profiles exhibited in the *Swift/XRT* data are variable, showing double peaks at the early stage and then merging into the single peak at the low luminosity. Additionally, we report that a low temperature ($kT \sim 0.1$ keV) thermal component emerges in the phase-averaged spectra as the flux decays, and it could arise from the outer truncated disk or the boundary layer.

Keywords: accretion, accretion disks — stars: neutron — pulsars: general — X-rays: binaries — X-rays: individual (SMC X-3)

1. INTRODUCTION

High-mass X-ray binaries contribute a large fraction of X-ray emission in normal galaxies, and they are believed to reflect the recent star-formation activity in the host galaxy (e.g. Grimm et al. 2002; Mineo et al. 2012). According to the status of the optical companion, high-mass X-ray binaries can be subdivided into supergiant X-ray binaries and Be/X-ray binaries (BeXBs). BeXB consists of a Be star and a compact object. Virtually, all confirmed compact object in BeXBs are neutron stars (NSs), and all these systems show X-ray pulsations (see Reig 2011 for reviews). As young systems, NSs in BeXBs have high magnetic field ($B > 10^{10}$ G); therefore, BeXBs provide unique natural laboratories for the study on extreme strong gravity and magnetic field physics.

The direct measurement of a NS magnetic field strength can be achieved from the detection of a cyclotron scattering resonance feature (e.g. Coburn et al. 2002; Yan et al. 2012; Fürst et al. 2014; Walter et al. 2015, and references therein). Additionally, investigating the interaction between the magnetosphere and the accretion matter, we can acquire the information of NS magnetic field indirectly (e.g. Weng & Zhang 2011; Shi et al. 2015; Christodoulou et al. 2016). That is, the strength of magnetic field can be illustrated by the size of magnetosphere co-rotating with the central NS. The boundary of magnetosphere is determined where the ram pressure of in-falling flow is balanced by magnetic pressure; thus, it expands with field strength and decreases with mass accretion rate (Lamb et al. 1973; Ghosh & Lamb 1979).

As the accretion rate decreases below the critical value,

the magnetospheric radius (R_m) grows beyond the corotation radius ($R_{co} = \sqrt[3]{\frac{GM P^2}{4\pi^2}}$), at which the Keplerian angular frequency is equal to the NS spin frequency, and the centrifugal barrier spins away accretion matter. If most of material is prevented from accreting onto NS, X-ray flux and pulsation decay sharply in a few days, i.e. the “propeller” effect (e.g. Cui 1997; Campana et al. 2014). Alternatively, the magnetosphere is penetrated into the corotation radius at the high luminosity, leading to the spin-up of NS. If NSs are close to spin equilibrium, their magnetic field can be estimated from long-term average spin parameters and X-ray luminosity (e.g. Klus et al. 2014; Shi et al. 2015). Meanwhile, the torque reversals between steady spin-up and spin-down are commonly shown in BeXBs (e.g. Bildsten et al. 1997).

Besides the long-term average spin evolution, the instantaneous torque measurements during episodic outbursts are essential to test accretion torque theories. Transient BeXBs experience periodic and less energetic ($L_X < 10^{37}$ erg/s) outbursts or rare giant outbursts, which are referred to as type I and type II outbursts, respectively (Reig 2011). The tight relationships between spin-up rate and (pulsed) flux detected in the luminous outbursts of BeXBs (e.g. A0535+262 and 2S 1417-624) are interpreted as the sign of transient accretion disks around NSs, which are supported by the simultaneous quasi-periodic oscillations (QPOs) detection (Finger et al. 1996; Sartore et al. 2015). It is worth to note that a small number of sources (e.g. SMC X-1, LMC X-4, 4U 0115+63, V0332+53) can reach the peak X-ray luminosity in excess of 10^{38} erg/s (e.g. Li et al. 2011; Mushtukov et al. 2015, and references therein). Intriguingly, a growing number of ultraluminous X-ray sources

(ULXs) in the nearby galaxies have been found to exhibit coherent pulsations (Bachetti et al. 2014; Fürst et al. 2016; Israel et al. 2016), indicating a connection to X-ray pulsars (Shao & Li 2015; Mushtukov et al. 2015). Nowadays, the super-Eddington accretion in magnetized NSs draw more extensive attention (e.g. Ekşi et al 2015; Pan et al. 2016; Tsygankov et al. 2016; Chen 2017). However, a detailed study on such dramatic phenomena is hampered by the lack of observation.

The Small Magellanic Cloud (SMC) is the second nearest galaxy ($d = 62.1$ kpc; Hilditch et al. 2005; Graczyk et al. 2014) after the The Large Magellanic Cloud, and it has high-mass X-ray binaries in abundance due to the recent star-forming activity (Zaritsky et al. 2002; Sturm et al. 2013). SMC X-3 (also known as SXP 7.78) was discovered with *SAS 3* X-ray observatory in 1978 (Clark et al. 1978), and was identified as an accreting pulsar with a 7.78 second pulsation detected (Edge et al 2004). The spectral type of the optical counterpart is identified as B1–B1.5 with $V = 14.91$ (McBride et al. 2008). The orbital period ~ 44.9 days was detected in both X-ray and optical bands (Galache et al. 2008; Bird et al. 2012). However, its eccentricity and the other orbital parameters are still unknown. Recently, SMC X-3 underwent a giant type II outburst in 2016 with a peak X-ray luminosity of $\sim 10^{39}$ erg/s, and it was monitored in Target of Opportunity mode by *Swift* since 2016 August 10. On 2016 November 8, we reported our preliminary results on analyzing the *Swift* data (Weng et al. 2016), which are the basis of this work. During preparation of this manuscript, Townsend et al. (2017, submitted) investigated the optical and X-ray data (including the *Swift* data) of SMC X-3, and obtained the similar orbital parameters of the binary as given in our paper. In this paper, we focus on the *Swift* data and carry out a comprehensive analysis on these data to investigate the physics of super-Eddington accretion in the magnetized NS. The data reduction is described in next section. In Section 3, we perform the timing analysis and calculate the orbital elements of the binary. In Section 4, we discuss the physical implications of these results and present main conclusions.

2. DATA REDUCTION

SMC X-3 triggered the *MAXI/GSC* on 2016 August 8 (Negoro et al. 2016) and was confirmed by *Swift* during it surveyed the SMC (Kennea et al. 2016). In this paper, we analyze all *Swift* pointing observations taken between 2016 August 10 and 2017 January 1. The *Swift* Gamma Ray Burst Explorer carries three scientific instruments covering a broad energy range of ~ 0.002 –150 keV: the Burst Alert Telescope (BAT), the X-ray Telescope (XRT), and the UV/Optical Telescope (UVOT) (Gehrels et al. 2004). The BAT daily light curve is adopted from Krimm et al. (2013)¹. Meanwhile, both the XRT and the UVOT data are processed with the packages and tools available in HEASOFT 6.19.

For the XRT data, the initial event cleaning is executed with the task `xrtpipeline` using standard quality cuts. The source events are extracted from a circle with a radius of 25 pixels centered at the source position, and an annulus region is adopted for background re-

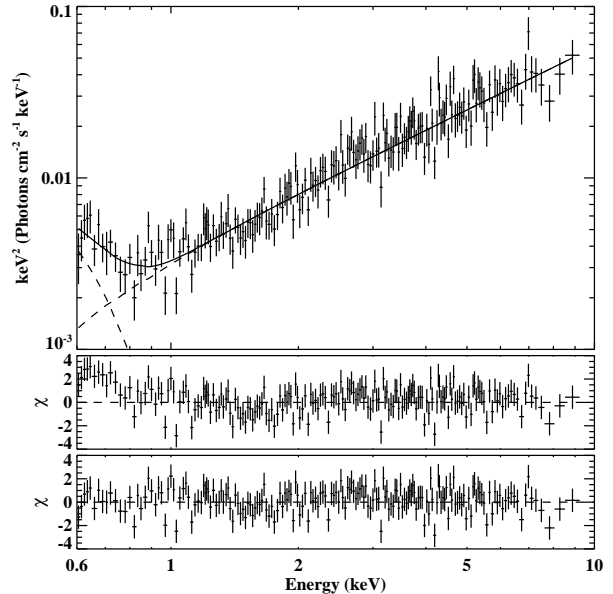


Figure 1. An example of X-ray spectrum observed on 2016 November 30 (ObsID = 00034673055). We fit the spectrum with a single PL model and the (BB+PL) model, and plot the residuals in the middle and the bottom panels, respectively. When the spectrum is fitted by a single absorbed PL model, a soft excess is clearly detected below 1 keV (middle panel). In the upper panel, we plot the unfolded spectrum for the (BB+PL) fitting.

gion. The light curves are corrected for the telescope and point-spread-function losses with the task `xrtlccorr`, and then are subtracted the scaled background count rate to yield the net light curves (Figure 2). The hardness for each observation is calculated as the ratio of average count rates (CR) in (2.0–10.0 keV)/(0.5–2.0 keV) bands. The ancillary response files are created using the task `xrtmkarf` and the latest response files (v015) are taken from the CALDB database for the spectral analyses. The spectral fitting is restricted to the 0.6–10 keV energy range due to calibration residuals below 0.6 keV for the windowed-timing mode data². The absorption column density along the line of sight to SMC X-3 is difficult to be constrained and could yield an extreme small value ($nH < 10^{14}$ cm⁻²) for part of observations; therefore, we fix it to 6.57×10^{20} cm⁻² (Dickey & Lockman 1990). At the early stage of outburst, the phase-averaged spectra can be well fitted by an absorbed power-law (PL) model with a photon index of ~ 0.9 –1.2. Around the end of September, the soft excess emerges below 1 keV (Figure 1), which can be described by a black-body (BB) emission with $kT \sim 0.1$ keV and $R_{BB} \sim 10^3$ km. However, because of the low S/N ratio of band-limited data, we cannot put an effective constraint on this component.

In addition to the pointing data, we involve the 17 survey observations (on the SMC) with an average exposure of ~ 60 s for the following photometry. For each observation, we first sum sky images with `uvotimsum`, and then perform aperture photometry with the summed images by using `uvotsource`. A source aperture of radius 5 arcsec and a larger neighbouring source-free region for

¹ <http://swift.gsfc.nasa.gov/results/transients/>

² see <http://swift.gsfc.nasa.gov/docs/heasarc/caldb/swift/docs/xrt/SWIFTXRT-CALDB-09.pdf>

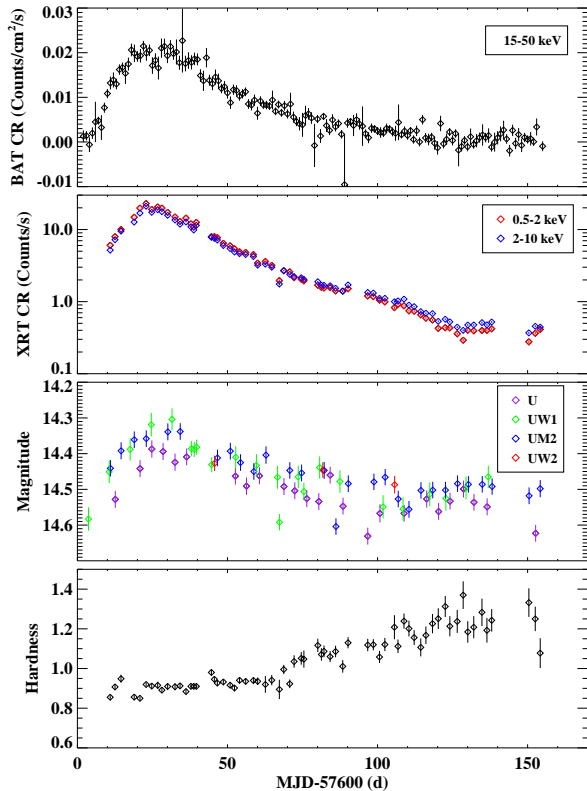


Figure 2. Panels from top to bottom show the light curves from the BAT, XRT, UVOT data, and the evolution of the 2–10 keV to 0.5–2 keV hardness ratios, respectively.

background are used. The AB magnitudes for all filters are shown in Figure 2.

3. TIMING ANALYSIS & RESULTS

The spin evolution during giant outbursts is crucial for investigating the accretion processes in BeXBs and for the determination of orbital parameters by using the orbital *Doppler* effect (e.g. Li et al. 2011). Before computing the spin frequency, we apply the barycentric correction with the `ftool barycorr` to the source event files (in the range of 0.5–10 keV). The spin frequency is obtained by folding the observed counts to reach the maximum Pearson χ^2 . The derived values of observed spin frequency are the same as presented by the *Fermi*/GBM Pulsar Project³; however, the source becomes faint and below the detection limit of GBM after MJD 57671 (Figure 3). After the frequency determined, the pulse profile is folded with the best frequency. For the purpose of comparing the profiles between observations, the pulse profiles are aligned by the cross correlation function.

3.1. Orbital Elements

To study the frequency evolution, the *Doppler* effects of the binary should be considered here. We use 7 frequency derivatives to fit the pulsar spin evolution as the spin frequency evolves quickly. The fitting is based on the Levenberg-Marquardt algorithm for nonlinear least

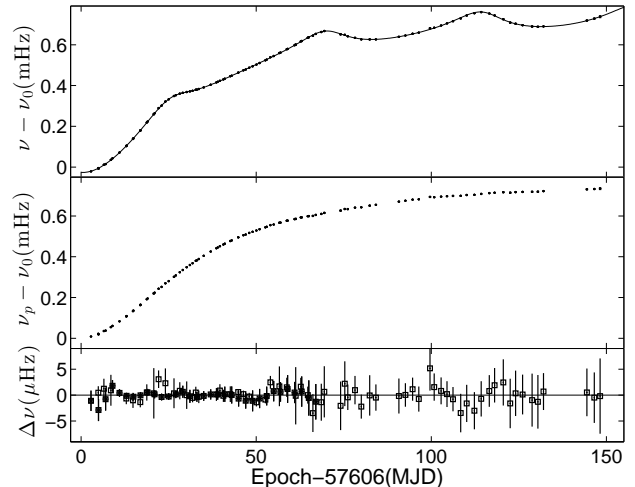


Figure 3. The spin frequencies without the orbital correction are plotted versus time (begin time: MJD 57606) in upper panel ($\nu_0 = 0.128\text{Hz}$), while the frequencies shown in middle panel have been orbitally corrected. The bottom panel shows fitting residuals of the spin and orbital parameters. The filled square data are adopted from the *Fermi*/GBM results.

Table 1

The timing results of SMC X-3 from the X-ray Observations

Parameters	Value
R.A.	$00^{\text{h}}52^{\text{m}}05^{\text{s}}.64$
Decl.	$-72^{\circ}26'04''.2$
Epoch(MJD)	57606
ν (mHz)	128.006(2)
$\dot{\nu}$ (10^{-5}Hz d^{-1})	-0.13(6)
$\ddot{\nu}$ (10^{-6}Hz d^{-2})	2.12(9)
ν_3 (10^{-7}Hz d^{-3})	-1.92(9)
ν_4 (10^{-9}Hz d^{-4})	1.1(7)
ν_5 (10^{-10}Hz d^{-5})	-4.0(3)
ν_6 (10^{-12}Hz d^{-6})	-9.3(9)
ν_7 (10^{-13}Hz d^{-6})	-1.0(1)
Porb(d)	44.53(8)
asini(light-second)	194(1)
e	0.262(4)
ω°	202(2)
T_{ω} (MJD)	57632.1(2)

square method, weighted by the error of each point, which is similar with the fitting process described in Li et al. (2011, and references therein). The errors of parameter are calculated from the covariance matrix of the parameter estimates. The best fitted parameters listed in Table 1 are quite consistent with those reported in Townsend et al. (2017).

It is difficult to obtain the derivative of spin frequency with the individual observation. Alternatively, we calculate the spin-up rates from the fitting results and the X-ray fluxes for each two successive observations, and plot them in Figure 5.

4. DISCUSSION & CONCLUSIONS

During the 2016 giant outburst, the X-ray luminosity of SMC X-3 reaches a peak value $\sim 10^{39}$ erg/s (in 0.5–10 keV) around August 24, that is a few times of NS Eddington luminosity and close to the low-luminosity tail of ULXs. The BAT daily light curve shows an indication of

³ <http://gammaray.nsstc.nasa.gov/gbm/science/pulsars.html>

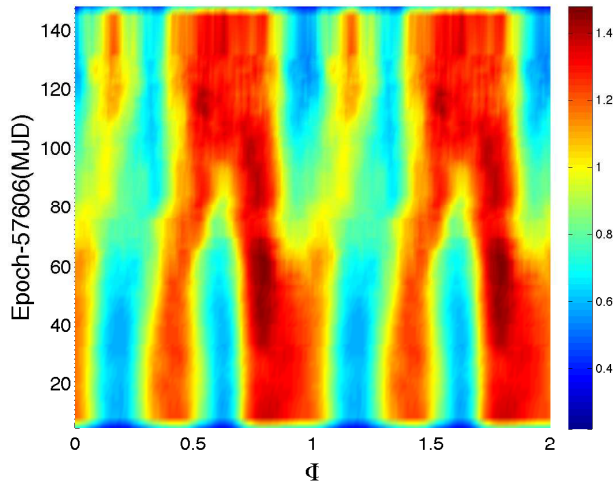


Figure 4. Evolution of the normalized pulse profiles. The color bar marks the normalized CR.

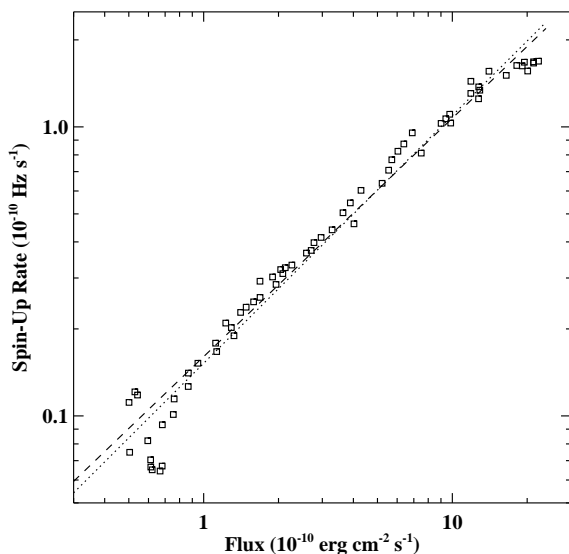


Figure 5. Relationship between the 0.5-10 keV unabsorbed flux and the spin-up rate during the 2016 super-Eddington outburst. The dashed line is best-fit power-law with a index of 0.82 ± 0.02 , and the dotted line is power-law with the expected index of $6/7$.

flat plateau during $\text{MJD} \sim 57618 - 57640$. In the meantime, the magnitudes in optical/near-ultraviolet bands increase by $\sim 0.2^m - 0.3^m$. Its X-ray spectra become harder as flux decays (Figure 2).

According to the *Doppler* motion of the binary, we fit the orbital modulation of the observed pulse period, obtain an orbital period of $P = 44.53 \pm 0.08$ days which is consistent with the previous works (Galache et al. 2008; Bird et al. 2012), and determine the projected semi-major axis $asini = 194 \pm 1$ light seconds and an eccentricity of $e = 0.262 \pm 0.004$. After correcting for the orbital motion, we find that the spin frequency increases steadily indicating the formation of a transient accretion disk surrounding the central NS during the outburst. According

to the accretion torque theory, we would expect the spin-up rate increases with the accretion rate ($\dot{\nu} \propto \dot{M}^{6/7}$) (Ghosh & Lamb 1979; Wang 1981). The power-law relationships between $\dot{\nu}$ and X-ray luminosity have been confirmed in some BeXBs during their type II giant outbursts and consistent with the results of QPOs evolution (e.g. Finger et al. 1996; İcđem et al. 2011; Sartore et al. 2015). However, the fitted power-law indexes are generally greater than the prediction of $6/7$. Alternatively, fitting the spin-up rate and the 0.5–10 keV flux of SMC X-3 with a power-law, we obtain an index of 0.82 ± 0.02 being close to $6/7$, but the relation deviates from the power-law at the peak and the low luminosity (Figure 5).

Klus et al. (2014) investigated all *RXTE*/PCA data to determine the long-term average spin period ($P = 7.7836 \pm 0.0001$), spin-down rate ($\dot{P} = 0.00262 \pm 0.00003 \text{ s yr}^{-1}$), and the average X-ray luminosity ($L_X \sim 3.7 \times 10^{36} \text{ erg/s}$) for SMC X-3. These results point to a torque switch from spin-down to spin-up at the beginning of the giant outburst ($L_X < 10^{38} \text{ erg/s}$). By assuming spin equilibrium, they derived a magnetic field of $\sim 2.9 \times 10^{12} \text{ G}$. Here, we report the instantaneous spin period measurements during the 2016 giant outburst. The spin frequency with the orbital correction evidently is evidently near the torque equilibrium with the spin frequency derivative close to zero at a luminosity of $\sim L_X \sim 2.3 \times 10^{37} \text{ erg/s}$ assuming the distance of 62.1 kpc (Figures 3 and 5). Thus, we can estimate a magnetic field of SMC X-3 with the assumption of $R_{\text{co}} = R_m$, or $B = [4.8 \times 10^{10} P^{7/6} (\frac{\text{flux}}{10^{-9} \text{ erg cm}^{-2} \text{ s}^{-1}})^{1/2} \times (\frac{d}{1 \text{ kpc}}) \times (\frac{M}{1.4 M_\odot})^{1/3} \times (\frac{R}{10^6 \text{ cm}})^{-5/2}] \text{ G}$ for the simplified model (Cui 1997), yielding $B \sim 7.3 \times 10^{12} \text{ G}$. That is, the obtained value is significantly higher than that reported by Klus et al. (2014). Intriguingly, if taking the color correction factor into account, the emission size of the thermal component detected during the source returning to the quiescence state is close to the corotation radius of SMC X-3 ($R_{\text{co}} \sim 6000 \text{ km}$). It further supports the torque equilibrium hypothesis, although the *Swift* data are still not good enough at the soft X-ray band to make a solid conclusion.

At the low luminosity, the single peak pulse profiles were exhibited in the *RXTE* (Galache et al. 2008), *Chandra* and *XMM-Newton* archival data (Haberl et al. 2008), which are executed more than ten years ago. As shown explicitly in Figure 4, the pulse profiles of SMC X-3 during the 2016 outburst are variable and have double peaks at the beginning of the outburst, and then converges to a single peak as the flux decays below $L_X \sim 4 \times 10^{37} \text{ erg/s}$. The similar evolution pattern of pulse profiles has been reported in other outbursts but with lower transient luminosity, e.g. the 1994 giant outburst of A0535+262 (Bildsten et al. 1997). These results can be interpreted as different geometries of the accretion column at beyond and below the critical luminosity ($\sim 10^{37} \text{ erg/s}$; e.g. Becker et al. 2012; Sartore et al. 2015), respectively. At lower luminosity, the in-falling gas may be decelerated via Coulomb interactions and a pencil-beam of emission is formed. At the supercritical state, the accretion flow is decelerated via the radiative shock and the photons can only escape from accretion column

walls resulting in double peaks structure (i.e. fan beam mode; e.g. Becker et al. 2012). It is worth to note that all three accreting NSs found in the ULXs have higher X-ray luminosity but present the single peak pulse profiles (Bachetti et al. 2014; Fürst et al. 2016; Israel et al. 2016). We suggest that the discrepancies between the pulse profiles exhibited in three ULXs and the super-Eddington outburst of SMC X-3 cannot be simply ascribed to different viewing angles, but might due to the different radiation mechanism having different geometry.

S.S.W. thanks Dr. Kim Page from *Swift* team for discussions on data analysis. We thank Jian Li and Xiao-Chuan Jiang for many valuable suggestions. This work is supported by the National Natural Science Foundation of China under grants 11303022, 11133002, 11573023, 11173016, 11673013, 11503027 and 11433005, and by the Special Research Fund for the Doctoral Program of Higher Education (grant No. 20133207110006).

REFERENCES

- Bachetti, M., Harrison, F. A., Walton, D. J., et al. 2014, *Nature*, 514, 202
- Becker, P. A., Klochkov, D., Schönherr, G., et al. 2012, *A&A*, 544, A123
- Bildsten, L., Chakrabarty, D., Chiu, J., et al. 1997, *ApJS*, 113, 367
- Bird A. J., Coe M. J., McBride V. A., & Udalski A., 2012, *MNRAS*, 423, 3663
- Campana, S., Brivio, F., Degenaar, N., et al. 2014, *MNRAS*, 441, 1984
- Chen, W.-C., 2017, *MNRAS*, 465, L6
- Christodoulou, D. M., Laycock, S. G. T., Yang, J., & Fingerman, S. 2016, *ApJ*, 829, 30
- Clark, G., Doxsey, R., Li F., Jernigan, J. G., & van Paradijs, J. 1978, *ApJ*, 221, L37
- Coburn, W., Heindl, W. A., Rothschild, R. E., et al. 2002, *ApJ*, 580, 394
- Cui, W. 1997, *ApJ*, 482, L163
- Dickey, J. M., & Lockman, F. J. 1990, *ARA&A*, 28, 215
- Edge, W. R. T., Coe, M. J., Corbet, R. H. D., Markwardt, C. B., & Laycock, S. 2004, *Astron. Telegram*, 225, 1
- Eksi, K. Y., Andaç, İ. C., Çikintoğlu, S., et al. 2015, *MNRAS*, 448, L40
- Finger, M. H., Wilson, R. B., & Harmon, B. A. 1996, *ApJ*, 459, 288
- Fürst, F., Pottschmidt, K., Wilms, J., et al. 2014, *ApJ*, 780, 133
- Fürst, F., Walton D.J., Harrison F.A., et al., 2016, *ApJL*, 831, L14
- Galache, J.L., Corbet, R.H.D., Coe, M.J., et al. 2008, *ApJS*, 177, 189
- Gehrels, N., Chincarini, G., Giommi, P., et al. 2004, *ApJ*, 611, 1005
- Ghosh, P., & Lamb, F. K. 1979, *ApJ*, 234, 296
- Goodman, J., & Weare, J., 2010, *camcos*, 5, 1
- Graczyk, D., Pietrzyński, G., Thompson, I. B., et al. 2014, *ApJ*, 780, 59
- Grimm, H. J., Gilfanov, M., & Sunyaev, R. 2002, *A&A*, 391, 923
- Haberl F., Eger P., Pietsch W., 2008, *A&A*, 489, 327
- Hilditch, R. W., Howarth, I. D., & Harries, T. J. 2005, *MNRAS*, 357, 304
- Hogg, D. W., Bovy, J., & Lang, D. 2010, arXiv:1008.4686
- İçdem, B., İnam, S., & Baykal, A. 2011, *MNRAS*, 415, 1523
- Israel, G.L., Belfiore, A., Stella, L., et al., 2016, arXiv:1609.07375
- Kennea, J. A., Coe, M. J., Evans, P. A., et al., 2016, *Astron. Telegram*, 9362, 1
- Klus, H., Ho, W. C. G., Coe, M. J., Corbet, R. H. D., & Townsend L. J., 2014, *MNRAS*, 437, 3863
- Krimm, H. A., Holland, S. T., Corbet, R. H. D., et al. 2013, *ApJS*, 209, 14
- Li, J., Wang, W., & Zhao, Y. H. 2011, *MNRAS*, 423, 2854
- Lamb, F. K., Pethick, C. J., & Pines, D. 1973, *ApJ*, 184, 271
- McBride, V.A., M.J. Coe, I. Negueruela, I., Schurch, M. P. E. & McGowan, K. E., 2008, *MNRAS*, 388, 1198
- Mineo, S., Gilfanov, M., & Sunyaev, R. 2012, *MNRAS*, 419, 2095
- Mushtukov, A. A., Suleimanov, V. F., Tsygankov, S. S., & Poutanen, J. 2015, *MNRAS*, 454, 2539
- Negoro, H., et al., 2016, *Astron. Telegram*, 9348, 1
- Pan, Y.Y., Song, L. M., Zhang, C. M., & Tong, H. 2016, *MNRAS*, 461, 2
- Reig, P., 2011, *Ap&SS*, 332, 1
- Sartore, N., Jourdain, E., & Roques, J.-P. 2015, *ApJ*, 806, 193
- Shao, Y., & Li, X.-D., 2015, *ApJ*, 802, 131
- Shi, C.-S., Zhang, S.-N., & Li, X.-D. 2015, *ApJ*, 813, 91
- Sturm, R., Haberl, F., Pietsch, W., et al. 2013, *A&A*, 558, A3
- Townsend, L. J., Kennea, J. A., Coe, M. J., et al., 2017, arXiv:1701.02336
- Tsygankov, S. S., Mushtukov, A. A., Suleimanov, V. F., & Poutanen, J. 2016, *MNRAS*, 457, 1101
- Walter, R., Lutovinov, A. A., Bozzo, E., & Tsygankov, S. S. 2015, *A&A Rev.*, 23, 2
- Wang, Y.-M. 1981, *A&A*, 102, 36
- Weng, S.-S., Ge, M.-Y., Zhao, H.-H., Wang, W., & Zhang, S.-N. 2016, *Astron. Telegram*, 9731, 1
- Weng, S.-S., & Zhang, S.-N. 2011, *ApJ*, 739, 42
- Yan, J.-Z., Chaty, S., Zurita Heras, J. A., Li, H., & Liu, Q.-Z., 2012, *ApJ*, 753, 73
- Zaritsky, D., Harris, J., Thompson, I. B., Grebel, E. K., & Massey, P. 2002, *AJ*, 123, 855